Molecular Therapy
Nucleic Acids
Original Article

Exon skipping induces uniform dystrophin rescue with dose-dependent restoration of serum miRNA biomarkers and muscle biophysical properties

Katarzyna Chwalenia,[1,2,7] Jacopo Oieni,[1,7] Joanna Zemła,[3] Małgorzata Lekka,[3] Nina Ahlskog,[1,2] Anna M.L. Coenen-Stass,[4,6] Graham McClorey,[1] Matthew J.A. Wood,[1,2,5] Yulia Lomonosova,[1,2,5,8] and Thomas C. Roberts[1,2,5,8]

[1]Department of Paediatrics, University of Oxford, South Parks Road, Oxford OX1 3QX, UK; [2]Institute of Developmental and Regenerative Medicine, University of Oxford, IMS-Tetsuya Nakamura Building, Old Road Campus, Roosevelt Drive, Headington, Oxford OX3 7TY, UK; [3]Department of Biophysical Microstructures, Institute of Nuclear Physics, Polish Academy of Sciences, PL-31342 Kraków, Poland; [4]Department of Physiology, Anatomy and Genetics, University of Oxford, South Parks Road, Oxford OX1 3QX, UK; [5]MDUK Oxford Neuromuscular Centre, South Parks Road, Oxford OX1 3QX, UK

Therapies that restore dystrophin expression are presumed to correct Duchenne muscular dystrophy (DMD), with antisense-mediated exon skipping being the leading approach. Here we aimed to determine whether exon skipping using a peptide-phosphorodiamidate morpholino oligonucleotide (PPMO) conjugate results in dose-dependent restoration of uniform dystrophin localization, together with correction of putative DMD serum and muscle biomarkers. Dystrophin-deficient *mdx* mice were treated with a PPMO (Pip9b2-PMO) designed to induce *Dmd* exon 23 skipping at single, ascending intravenous doses (3, 6, or 12 mg/kg) and sacrificed 2 weeks later. Dose-dependent exon skipping and dystrophin protein restoration were observed, with dystrophin uniformly distributed at the sarcolemma of corrected myofibers at all doses. Serum microRNA biomarkers (i.e., miR-1a-3p, miR-133a-3p, miR-206-3p, miR-483-3p) and creatinine kinase levels were restored toward wild-type levels after treatment in a dose-dependent manner. All biomarkers were strongly anti-correlated with both exon skipping level and dystrophin expression. Dystrophin rescue was also strongly positively correlated with muscle stiffness (i.e., Young's modulus) as determined by atomic force microscopy (AFM) nanoindentation assay. These data demonstrate that PPMO-mediated exon skipping generates myofibers with uniform dystrophin expression and that both serum microRNA biomarkers and muscle AFM have potential utility as pharmacodynamic biomarkers of dystrophin restoration therapy in DMD.

INTRODUCTION

Duchenne muscular dystrophy (DMD) is an X-linked, monogenic muscle-wasting disorder and the most common inherited myopathy affecting children. DMD is caused by loss-of-function mutations in the gene encoding dystrophin (*DMD*), which performs structural and signaling functions at the sarcolemma.[1–3] The leading approach for treating DMD is exon skipping, whereby splicing of the *DMD* pre-mRNA is modulated using antisense oligonucleotides, such that the translation reading frame is corrected, and an internally truncated, partially functional quasi-dystrophin protein is produced.[4] At the time of writing (August 2022) there are four FDA-approved exon skipping drugs for DMD: eteplirsen, viltolarsen, golodirsen, and casimersen (all unconjugated phosphorodiamidate morpholino oligonucleotides [PMOs] designed for skipping of *DMD* exons 51, 53, 53, and 45, respectively).[5] However, the levels of dystrophin achieved in treated DMD patient muscle are very low (~1% of healthy levels).[6,7] Studies of dystrophin restoration therapies have primarily focused on the amount and quality of dystrophin protein expressed.[8] In contrast, the importance of correct dystrophin localization has been less well studied. Notably, recent work from our group,[9] and others,[10] has suggested that uniform dystrophin expression is an important factor in the success of dystrophin restoration therapies and the severity of dystrophinopathies, respectively. Furthermore, challenges in determining dystrophin expression (e.g., the requirement for invasive biopsy, whether a single biopsy is reflective of the overall musculature, and technical difficulties associated with accurate measurement of dystrophin expression) have motivated the search for alternative DMD biomarkers.[11] For example, extracellular microRNAs (ex-miRNAs) constitute one such class of minimally invasive biomarkers that may have utility in the context of DMD.[12] The leading candidate miRNA biomarkers for DMD are the myomiRs (muscle-enriched miRNAs that regulate myoblast proliferation and

Received 12 May 2022; accepted 19 August 2022;
https://doi.org/10.1016/j.omtn.2022.08.033.

[6]Present address: Merck KGaA, Frankfurter Strasse 250, 64293 Darmstadt, Germany

[7]These authors contributed equally

[8]These authors contributed equally

Correspondence: Thomas C. Roberts, Institute of Developmental and Regenerative Medicine, University of Oxford, IMS-Tetsuya Nakamura Building, Old Road Campus, Roosevelt Drive, Headington, Oxford OX3 7TY, UK.
E-mail: thomas.roberts@paediatrics.ox.ac.uk

differentiation),[13–16] consisting of miR-1a-3p, miR-133a-3p, and miR-206-3p. These myomiRs are highly upregulated in DMD patient serum[17,18] and in various dystrophic mouse models, including *mdx*,[17–21] *mdx52*,[22] dKO (dystrophin/utrophin double knockout),[23] and *mdx*^{4cv}.[24] In the *mdx* mouse, it has been reported that extracellular myomiRs (ex-myomiRs) are less variable than serum creatine kinase (CK),[19] the gold standard clinical chemistry biomarker for neuromuscular disease. Multiple other putative DMD biomarkers have been identified.[25,26] For example, we recently identified miR-483-3p as being enriched in dystrophic mouse serum.[9,18] It is currently not clear whether any of these additional miRNA biomarkers offers an advantage over serum myomiRs.

ex-myomiRs offer excellent discrimination between DMD patients and healthy controls,[17,18] suggesting they could be used to diagnose patients. However, the myomiRs have also been found to be elevated in the serum in multiple other neuromuscular conditions (including myotonic dystrophy, spinal muscular atrophy, and amyotrophic lateral sclerosis),[24,27–30] meaning that they are not specific biomarkers for DMD. Importantly, diagnosis of DMD is not currently a major clinical challenge. Instead, these ex-miRNAs may have utility as minimally invasive biomarkers for monitoring disease progression or response to therapy, a currently unmet clinical need.[11,12]

A single intravenous treatment of the *mdx* DMD mouse model with peptide-PMO (PPMO; designed to skip *Dmd* exon 23 and thereby rescue dystrophin expression) leads to restoration of ex-myomiRs toward wild-type levels.[9,18,20,21] Similarly, ex-myomiR levels in dystrophic mouse serum are restored to near-wild-type levels after treatment with the U1[17] and U7[23] small nuclear RNA expressed exon skipping systems. Importantly, we observed that treatment with two PPMO conjugates with different potencies resulted in different degrees of ex-myomiR restoration,[21] suggesting that ex-myomiR levels might be suitable for non-invasively assessing dystrophin levels in muscle. We further investigated this phenomenon using a genetic model (the *mdx-Xist*$^{\Delta hs}$ mouse) in which dystrophin is expressed at variable levels as a consequence of skewed X-chromosome inactivation.[31] We generated animals that expressed ~10%, ~20%, and ~35% of healthy dystrophin protein levels, but surprisingly, ex-myomiR levels were not correlated with dystrophin protein expression at all, and were instead elevated at levels similar to those of dystrophin-null *mdx* controls, regardless of dystrophin expression.[9] Importantly, dystrophin is expressed in a within-fiber patchy manner in the *mdx-Xist*$^{\Delta hs}$ model,[9,31] suggesting that a uniform pattern of sarcolemmal dystrophin is important for therapeutic correction. Here, we aimed to determine if PPMO-mediated exon skipping resulted in dose-dependent uniform dystrophin expression, ex-myomiR restoration, and correction of the biophysical properties of dystrophic muscle.

RESULTS

Dose-dependent dystrophin restoration in *mdx* muscle following PPMO treatment

Male *mdx* mice were treated with a single intravenous injection (via the tail vein) of a PPMO conjugate (Pip9b2-PMO) (Figures 1A and 1B) at 8 weeks of age. Mice were treated with one of three doses: 3 (n = 7), 6 (n = 9), or 12 mg/kg (n = 9). These treatments were intended to induce three different levels of dystrophin re-expression corresponding to each dose. Animals were sacrificed 2 weeks post treatment (i.e., at 10 weeks of age), at which point blood serum and tibialis anterior (TA) muscles were harvested. Untreated (age and sex matched) *mdx* (n = 9) and wild-type (WT; n = 5) animals were harvested in parallel as controls (Figure 1A). Dose-dependent restoration of dystrophin protein expression was confirmed by western blot with median expression values of 3.7%, 16.7%, and 44.8% of WT levels for the 3, 6, and 12 mg/kg PPMO-treatment groups, respectively (Figures 1C and 1D). Dystrophin protein was undetectable in untreated *mdx* TA muscle lysates (Figure 1C). The levels of exon-skipped (ΔExon23) *Dmd* transcripts in PPMO-treated muscle was similarly dose responsive (Figure 1E), as determined by RT-qPCR. Median skipped transcript levels were 1.2%, 11.8%, and 38% of total transcripts for the three PPMO-treatment dose groups, respectively. Dystrophin protein quantification and exon-skipped transcript levels were strongly correlated (Spearman's $r = 0.9262$, $p < 0.0001$, Figure 1F).

Validation of myomiR RT-qPCR assay specificity

The leading serum miRNA biomarkers in the context of DMD are the myomiRs,[12] consisting primarily of two miRNA families: (1) the miR-1/206 family (i.e., miR-1a-3p and miR-206-3p) and (2) the miR-133 family (i.e., miR-133a-3p and miR-133b-3p). miR-1a-3p and miR-206-3p share the same seed sequence and differ at only 4 nucleotides. Conversely, miR-133a-3p and miR-133b-3p are identical except for the 3'-terminal nucleotide (Figure 2A). Despite their sequence similarity, miR-133a-3p and miR-133b-3p are derived from distinct genomic loci and are expressed at different levels in murine muscle, with miR-133a-3p being ~5-fold more abundant than miR-133b-3p (Figure S1A).[18] The first report of serum myomiR levels in dystrophic serum commented that the RTq-PCR methodology used (miScript, developed by Qiagen) was unable to distinguish between miR-133a-3p and miR-133b-3p.[17] Since that initial report, several groups have reported serum miRNA quantification data for these two miRNAs in the context of DMD,[24,32–34] myotonic dystrophy,[30,35–37] and human fetal myogenesis.[38] These studies utilized the small-RNA TaqMan RT-qPCR method (from Applied Biosystems, now Thermo Fisher Scientific),[39] which involves an RNA-specific stem-loop primer in the reverse transcription (RT) step. The small-RNA TaqMan approach is by far the most widely adopted miRNA quantification technology at use in this field (Figure S2B, Table S1). We were therefore motivated to determine if these assays are sufficiently specific to distinguish between miR-1a-3p and miR-206-3p, and between miR-133a-3p and miR-133b-3p. To this end, we generated artificial samples consisting of 50 fmol solutions of synthetic single-stranded RNA oligonucleotide mimics of each miRNA (Table S2, IDT) in nuclease-free water. Each artificial sample contained a single type of miRNA and was subsequently subjected to RT using either the correct RT primer that corresponded to the respective miRNA or the incorrect RT primer that corresponded to the related off-target miRNA. The resulting cDNA was analyzed in separate reactions using both the on-target and the off-target qPCR

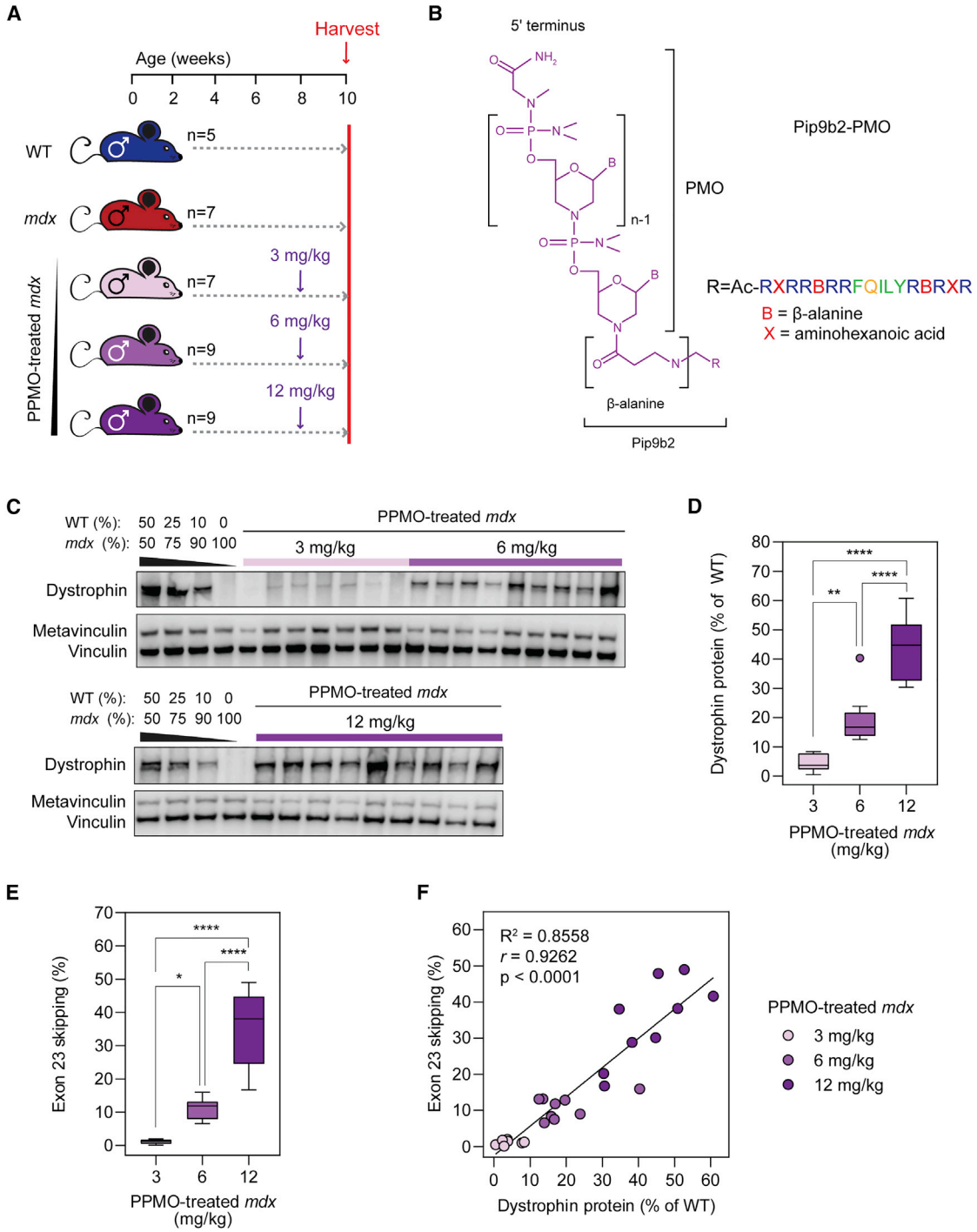

Figure 1. Dose-dependent dystrophin restoration in *mdx* mice treated with PPMO conjugates

(A) Schematic of experimental design. Eight-week-old male *mdx* mice were treated with a single intravenous injection of PPMO conjugate (at a dose of 3, 6, or 12 mg/kg) and harvested for analysis 2 weeks later. (B) Structure of the PPMO conjugate, which consists of a Pip9b2 peptide covalently conjugated to a PMO antisense oligonucleotide designed to skip *Dmd* exon 23. (C) Western blot of dystrophin protein expression for all PPMO-treated *mdx* TA muscle lysates. Vinculin was used as a loading control. (D) Tukey boxplot of dystrophin protein expression quantification. (E) Tukey boxplot of *Dmd* exon 23 skipping as determined by RT-qPCR. Statistical significance was tested by one-way ANOVA and Bonferroni *post hoc* test. *p < 0.05, **p < 0.01, ****p < 0.0001. (F) Correlation plot of dystrophin protein expression and exon 23 skipping levels for PPMO-treated *mdx* samples. Values were analyzed using linear regression and Spearman correlation analyses.

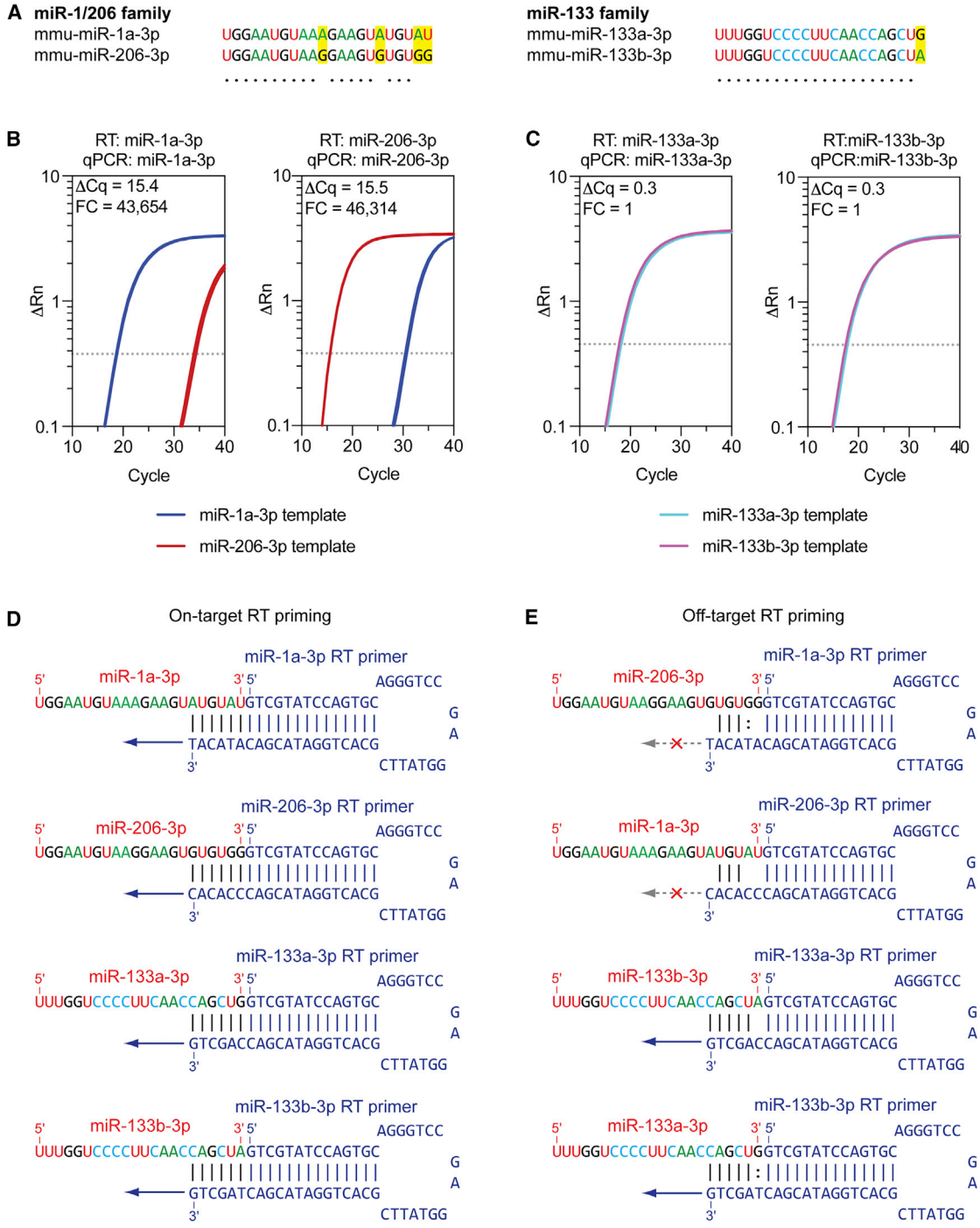

Figure 2. Stem-loop primed reverse transcription does not discriminate between miR-133a-3p and miR-133b-3p

(A) Sequence alignments for the miR-1/206 and miR-133 myomiR families. Differences between miRNA family members are highlighted in yellow. Artificial samples containing 50 fmol of synthetic miRNA mimic oligonucleotide templates were amplified using either the intended on-target small-RNA TaqMan assay (i.e., both RT primer and qPCR primer/probe mixes) or the assay for the related off-target miRNA. Amplification plots are shown for (B) miR-1a-3p and miR-206-3p and (C) miR-133a-3p and miR-133b-3p (the threshold is indicated by a dotted line). Diagrams of stem-loop reverse transcription primers in complex with either (D) their intended cognate target miRNA or (E) the unintended off-target related miRNA. High complementarity in the miRNA binding region for the miR-133 family stem-loop primers explains the off-target priming observed for miR-133a-3p and miR-133b-3p. FC, fold change.

assays. These experiments were designed to determine if (1) the RT primers can distinguish between closely related RNA targets and (2) whether the qPCR assays can distinguish between closely related cDNA templates.

Initially, each artificial sample was reverse transcribed with either the on-target or the closely related off-target RT primer, and then qPCR was performed using the correct qPCR assay. For the miR-1/206 family, the assays were found to be highly specific, with greater than 40,000-fold difference (ΔCq > 15.4) between on-target and off-target amplification (Figure 2B). Cq values for the off-target amplification were ~31–35, suggestive of low or very low levels of amplification. Conversely, the miR-133 family assays were not capable of discriminating between miR-133a and miR-133b, as equivalent amplification was observed when the miR-133a and miR-133b oligonucleotides were analyzed with either assay (ΔCq = 0.3) (Figure 2C). This lack of specificity could be attributed to the RT step, as negligible amplification was observed when the miRNA mimics were first reverse transcribed using the correct stem-loop primer, followed by qPCR with the off-target TaqMan assay (Figure S2). The reason for the cross-reactivity of these assays becomes apparent when the interactions between the stem-loop primers and the on-target/off-target miRNAs are inspected (Figures 2D and 2E). Stem-loop primers recognize their cognate miRNAs through the binding of the six 3'-terminal nucleotides of the RT primer with six complementary 3'-terminal nucleotides of the miRNA, which permits priming of the RT enzyme (Figure 2D). For off-target primer interactions for the miR-1/206 family miRNAs, there are either two or three mismatches between the RT primer and the miRNA, including at the most 3'-terminal nucleotide, which is unlikely to support priming (Figure 2D). Conversely, for the miR-133 family, there is only one mismatch or one wobble base pair between primer and miRNA for the off-target RT primer combinations, respectively. In particular, the most 3'-terminal nucleotide is complementary in both cases, which is expected to support priming and therefore explains the high levels of off-target miR-133 amplification (Figure 2E).

These data demonstrate that small-RNA TaqMan assays are unable to distinguish between miR-133a-3p and miR-133b-3p, and are unlikely to be able to discriminate between other small RNAs that differ only at the 3' terminus in the general case. For this reason, we have chosen not to investigate either miR-133a-3p or miR-133b-3p separately using RT-qPCR in our studies. Instead, we report only miR-133a-3p data (while acknowledging here that this assay will also amplify the less abundant miR-133b-3p species). Notably, we have previously shown that both miR-133a-3p and miR-133b-3p are upregulated in dystrophic serum using small-RNA sequencing (which can distinguish between these miRNAs).[18]

Dose-dependent ex-myomiR restoration in *mdx* serum following PPMO treatment

We next sought to analyze the serum levels of putative DMD biomarker myomiRs (miR-1a-3p, miR-133a-3p, miR-206-3p, and miR-483-3p) in the PPMO-treated animals, compared with WT and *mdx* controls. Levels of serum CK were measured in parallel. RNA was extracted from serum samples and miRNA levels were determined by small-RNA TaqMan RT-qPCR. All miRNA biomarkers were elevated in *mdx* serum (Figure 3). The myomiRs were significantly upregulated in *mdx* serum with median fold-change increases of 16-, 19.9-, and 48-fold for miR-1a-3p, miR-133a-3p, and miR-206-3p, respectively (Figures 3A–3C). miR-483-3p was upregulated by 12.5-fold but did not reach statistical significance at the $p < 0.05$ level (Figure 3D). PPMO-treated *mdx* mice exhibited a dose-dependent shift in all miRNA biomarkers toward WT levels. Specifically, the animals in the 12 mg/kg group exhibited biomarker restoration that was close to (and not significantly different from) WT levels, especially in the cases of miR-1a-3p and miR-133a-3p. Conversely, the animals in the 6 mg/kg group exhibited biomarker levels that were intermediate between those of *mdx* and WT animals (Figures 3A–3D). Highly similar results were observed for serum CK (Figure 3E). Notably, the variation in CK measurements was less than that observed for the miRNA biomarkers, and consequently more intergroup statistically significant changes were detected.

Ex-myomiR biomarkers are anti-correlated with dystrophin expression

Correlation analyses were performed to compare either muscle dystrophin expression or exon skipping levels with matched biomarker levels for PPMO-treated animals (Figure 4). Serum biomarker levels were strongly negatively correlated with dystrophin protein expression: miR-1a-3p, $r = -0.72$; miR-133a-3p, $r = -0.76$; miR-206-3p, $r = -0.64$; miR-483-3p, $r = -0.55$; and CK, $r = -0.75$ (all $p < 0.005$) (Figures 4A–4E). Similarly, serum biomarker levels were also strongly negatively correlated with exon 23 skipping: miR-1a-3p, $r = -0.67$; miR-133a-3p, $r = -0.75$; miR-206-3p, $r = -0.67$; miR-483-3p, $r = -0.64$; and CK, $r = -0.75$ (all $p < 0.0006$) (Figures 4F–4J). Conversely, the serum biomarkers were positively correlated with one another (Figure 4K, $r > 0.72$, $p < 5.2 \times 10^{-5}$). miR-133a-3p was the most strongly correlated biomarker compared with dystrophin protein (Figure 4B), with serum CK a close second (Figure 4E). In contrast, miR-483-3p was the most weakly correlated biomarker (Figures 4D and 4I).

Dose-independent uniform dystrophin distribution after PPMO treatment

We previously showed that dystrophin distribution is uniform after treatment with a single 12.5 mg/kg dose of Pip9b2-PMO in the *mdx* mouse.[9] This is in contrast to the patchy pattern of dystrophin expression observed in *mdx-Xist*$^{\Delta hs}$ mice expressing equivalent total levels of dystrophin compared with that achieved with exon skipping.[9] We were therefore motivated to assess whether a within-fiber uniform pattern of dystrophin expression is observed at all PPMO doses tested. To this end, we analyzed dystrophin expression by immunofluorescence staining in TA muscle sections in both transverse and longitudinal orientations (Figure 5). PPMO-treated *mdx* mice generally exhibited a uniform pattern of dystrophin expression. In the low-dose (3 mg/kg) group, some degree of between-fiber

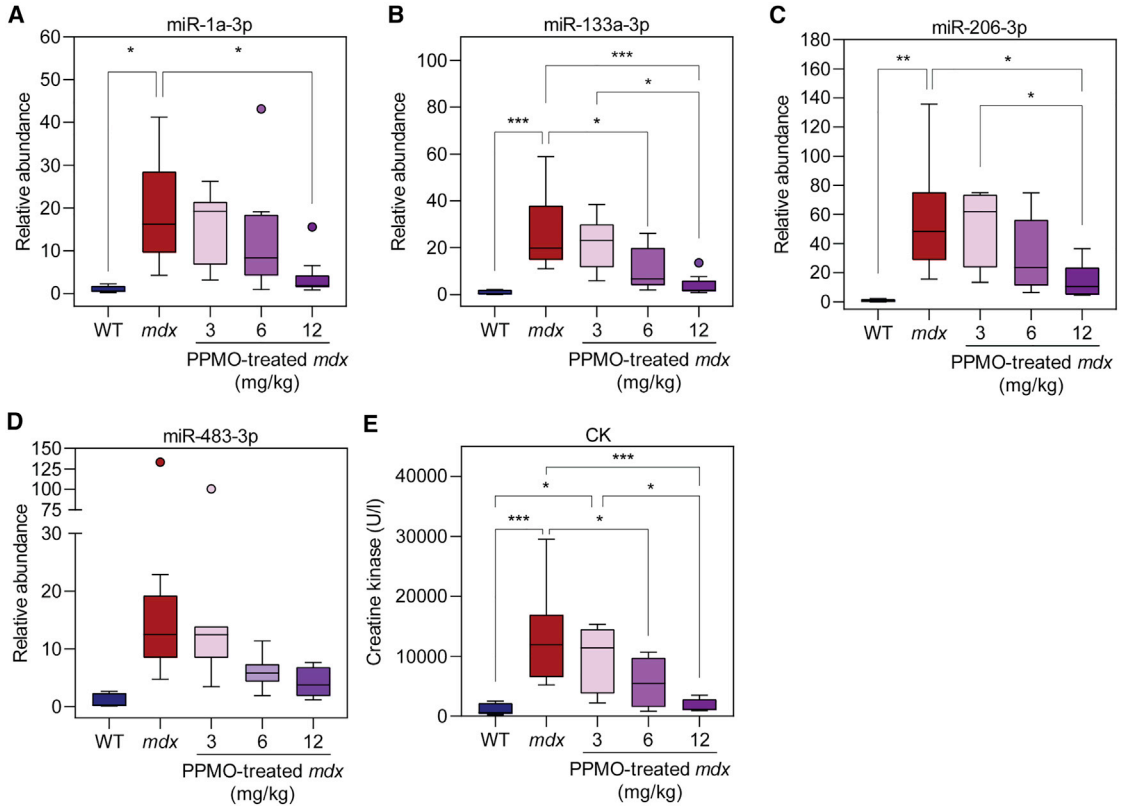

Figure 3. Extracellular myomiRs are pharmacodynamic biomarkers of exon-skipping-mediated dystrophin restoration

Eight-week-old male *mdx* mice were treated with a single intravenous injection of PPMO conjugate (Pip9b2-PMO) at one of three doses (3, 6, or 12 mg/kg). Mice were harvested 2 weeks after treatment (age 10 weeks) and serum was analyzed for (A) miR-1a-3p, (B) miR-133a-3p, (C) miR-206-3p, (D) miR-483-3p, and (E) creatine kinase (CK). Serum from untreated WT and *mdx* animals served as controls. Data are shown as Tukey boxplots, with statistically significant differences tested by one-way ANOVA with Bonferroni *post hoc* test, *$p < 0.05$, **$p < 0.01$, ***$p < 0.001$.

patchiness was observed when sections were viewed in transverse orientation (Figure 5). Specifically, some fibers were dystrophin positive, whereas others were dystrophin negative. The positively stained fibers generally exhibited consistent staining around the circumference of the fiber, although the strength of the staining was also weak in some fibers. In contrast, within-fiber patchiness was not observed, as viewed in longitudinal orientation (Figure 5).

Dose-dependent restoration of myofiber elasticity following PPMO treatment

A subset of the mice described above was further analyzed by atomic force microscopy (AFM) nanoindentation assay to investigate the relationship between dystrophin restoration, circulating biomarker levels, and the biophysical properties of muscle. AFM measures the resistance of a sample to an external deforming force, such that its stiffness can be determined.[40,41] To this end, TA muscle explants (all n = 4) from WT, *mdx*, and PPMO-treated *mdx* mice at the three doses, 3, 6, or 12 mg/kg, were assessed by AFM. Force versus displacement measurements were performed, and Young's modulus (E, a measure of the stiffness of the biological sample in response to an applied load) was calculated as described previously.[40] An indentation depth of 1,050 nm was utilized such that Young's modulus measurements reflected the stiffness of the myofiber inner structure, deeper than the actin microfilaments directly underlying the sarcolemma.

The mean E values were 4.7 and 1.7 kPa for the WT and *mdx* mice, respectively (a 2.7-fold reduction in *mdx* muscle, $p < 0.0001$), indicative of markedly lower resistance of dystrophic muscle to reversible deformation (Figure 6A), consistent with previous observations.[40,41] Treatment with PPMO resulted in a dose-dependent shift in the mean E values (Figure 6A). Young's modulus values were not significantly different between *mdx* mice treated with PPMO at the lowest dose, i.e., 3 mg/kg, and untreated *mdx* mice (Figure 6A), whereas the 6 mg/kg PPMO treatment was sufficient to completely reverse the reduction in stiffness observed in *mdx* muscle (Figure 6A). Interestingly, treatment with 12 mg/kg PPMO resulted in an ~2-fold increase ($p < 0.0001$) in Young's modulus (mean E = 9.2 kPa) relative to the WT control group, suggesting a higher resistance to the deformation compared with that in the control mice (Figure 6A). Very similar

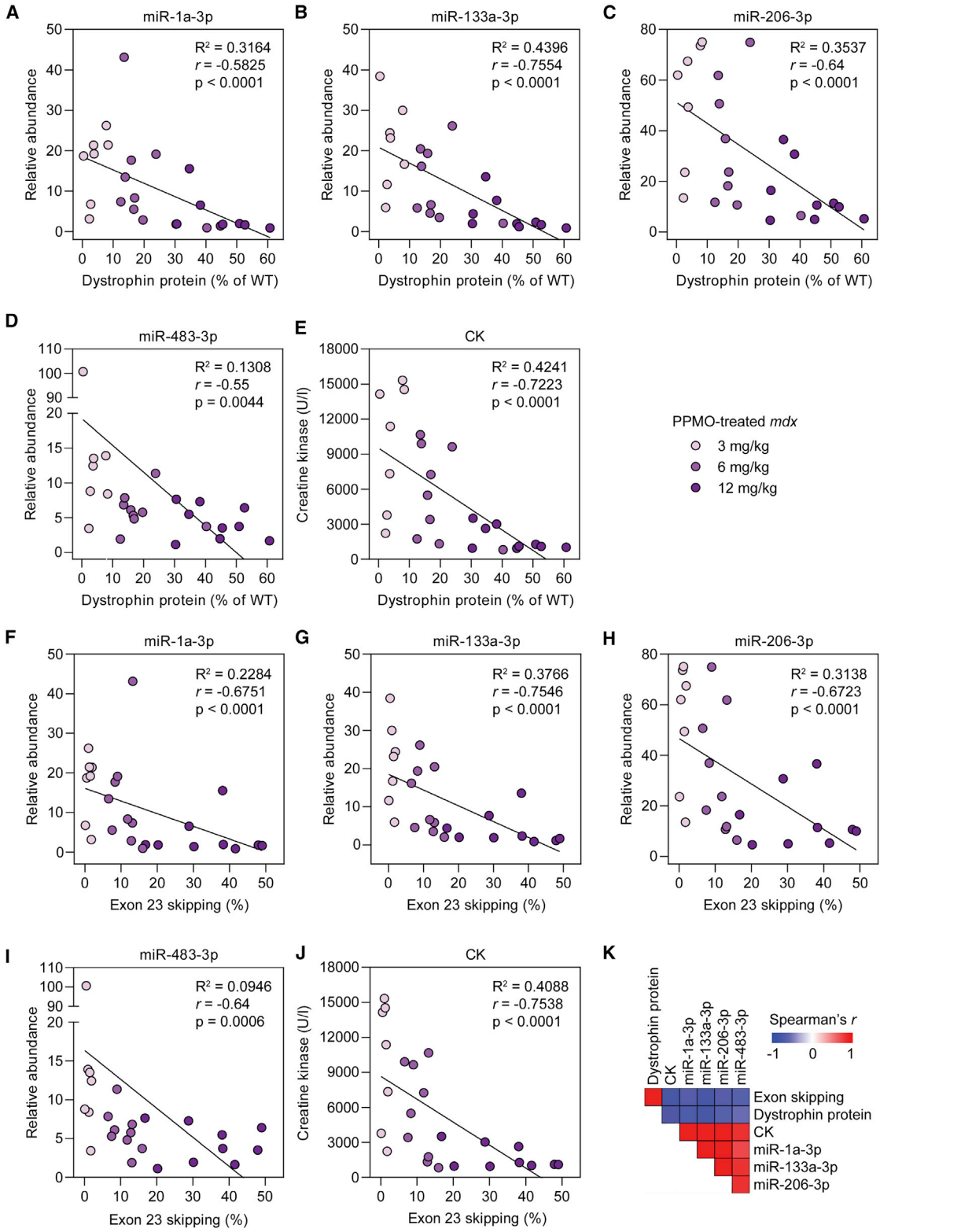

(legend on next page)

results were observed using measurement depths of 250 and 550 nm (Figure S3).

Inspection of underlying *E* value determinations revealed a Gaussian distribution in *mdx* muscle with an *E* maximum at 1–2 kPa, consistent with high myofiber elasticity (Figure 6B). WT *E* values exhibited a bimodal distribution with maxima at 2–3 and 7–8 kPa (Figure 6B). The PPMO-treated *mdx* samples showed a gradation of effect, whereby the distribution of *E* values shifted from an *mdx*-like distribution in the 3 mg/kg group to a more WT-like distribution in the 12 mg/kg group. For the low-dose 3 mg/kg group, the data were fit to a Gaussian distribution similar to the *mdx* samples, although a smaller population of measurements with *E* values ∼5–7 kPa was also observed, which did not fit the calculated distribution. The results obtained for the 6 and 12 mg/kg data were best fitted with the sum of two Gaussian distributions, although the 6 mg/kg data were monomodal and the 12 mg/kg data were bimodal. The distribution of *E* values in the high-dose group resembled that of WT muscle, although the *E* values were shifted to the right (with a maximum at 6–8 kPa) and there were a high proportion of stiffer measurements (including up to 14–15 kPa), indicating an increase in myofiber stiffness in the PPMO-treated samples relative to WT (Figure 6B). Mean Young's modulus was strongly positively correlated with both dystrophin protein expression ($r = 0.909$, $p < 0.0001$) (Figure 6C) and exon 23 skipping ($r = 0.902$, $p < 0.01$) (Figure 6D) in PPMO-treated *mdx* mice. Overall, these findings suggest that exon-skipping-mediated dystrophin rescue can restore the biophysical properties of dystrophic muscle.

DISCUSSION

Here we show that treatment of dystrophin-deficient *mdx* mice with Pip9b2-PMO results in dose-dependent *Dmd* exon 23 skipping, dystrophin rescue, restoration of circulating miRNA biomarker levels, and correction of muscle biophysical properties. Treatment of *mdx* mice with PPMO conjugates resulted in a within-fiber uniform pattern of sarcolemmal dystrophin expression across dose levels (Figure 5), consistent with our previous results.[9] This is in contrast to our observations in CRISPR-Cas9-treated muscle (see related article),[42] whereby dystrophin was expressed in a patchy manner. These findings point to a potential advantage of antisense oligonucleotide-mediated exon skipping over gene editing.[43]

This study adds to the growing body of literature that supports the use of ex-myomiRs as minimally invasive biomarkers for use in DMD patients. Notably, the negative correlations between circulating miRNA levels and molecular correction of dystrophin (Figure 4) suggest that these miRNAs could be utilized as pharmacodynamic biomarkers to assess the effectiveness of experimental therapies in clinical trials or approved therapies in patients. These findings are consistent with observations from a previous study from our group whereby two PPMO conjugates with differing potencies were found to induce corresponding levels of biomarker restoration.[21] Importantly, several lines of evidence indicate that ex-myomiRs are not biomarkers of dystrophin expression *per se*. First, the elevation of serum myomiR levels (i.e., miR-1, miR-133, and miR-206) has been reported in the context of multiple other myopathies,[28,35,44,45] and so is not a unique feature of dystrophinopathy. Second, serum myomiR biomarkers have been shown to be restored to WT levels in DMD mouse models following experimental therapies that do not involve dystrophin restoration. Specifically, serum miR-206 was restored to WT levels in *mdx* mice treated with a myostatin pathway blockade strategy (i.e., in the context of no dystrophin restoration),[46] and serum myomiRs are also present at WT levels in *mdx*-Fiona mice (which lack dystrophin but overexpress the dystrophin paralog utrophin).[47] Instead, we have suggested that ex-myomiR levels are reflective of muscle turnover (i.e., myonecrosis and compensatory regeneration) based on several lines of evidence: (1) ex-myomiRs are elevated during perinatal myogenesis in both WT and *mdx* animals,[48] (2) myomiRs are progressively released by human and murine myoblast cultures undergoing differentiation,[48] and (3) a biphasic pattern of ex-myomiR release was observed in *mdx* mice following an acute exercise regimen, corresponding to an initial damage phase immediately after exercise and a secondary regenerative phase 5–7 days post exercise.[48] Furthermore, there is a degree of selectivity in myomiRs release,[18,48] suggesting that passive leakage from damaged muscle is insufficient to explain their serum abundance levels. Work from our group in the *mdx* mouse has shown that ex-myomiRs are primarily non-vesicular and are instead protected from nucleolytic degradation through interactions with serum proteins.[21,49]

Analysis of the biophysical properties of muscle using an AFM nanoindentation assay revealed reduced resistance to mechanical deformation (i.e., stiffness) in dystrophic muscle (Figure 6), consistent with previous reports.[40,41] PPMO treatment restored myofiber elastic properties in a dose-responsive manner, although the high PPMO dose increased stiffness beyond that observed in WT mice. The reason for this is unclear, but given that treated *mdx* mice exhibit signs of muscle hypertrophy[9] (Figure 5), the resulting increase in the concentration of protein components of the contractile apparatus and cytoskeletal proteins may contribute to this increase in myofiber stiffness. In addition, the myonuclei of *mdx* myofibers are often arranged in centrally nucleated chains, indicative of recent regeneration events, which may also contribute to an increase in stiffness.[50] These data provide further evidence that serum miRNA measurements can be used to provide information about the underlying muscle (patho) physiology. Similarly, AFM has been used to assess the elastic properties of DMD patient biopsy material, suggesting that this technique

Figure 4. Serum biomarkers are strongly anti-correlated with dystrophin expression and exon 23 skipping levels in PPMO-treated *mdx* mice

Correlation analyses for dystrophin protein expression versus (A) miR-1a-3p, (B) miR-133a-3p, (C) miR-206-3p, (D), miR-483-3p, and (E) serum CK. Correlation analyses for *Dmd* exon 23 skipping versus (F) miR-1a-3p, (G) miR-133a-3p, (H) miR-206-3p, (I) miR-483-3p, and (J) serum CK. Values were analyzed using linear regression and Spearman correlation analyses. (K) Heatmap of Spearman correlation coefficients for all pairwise comparisons. Red indicates a positive correlation and blue indicates a negative correlation.

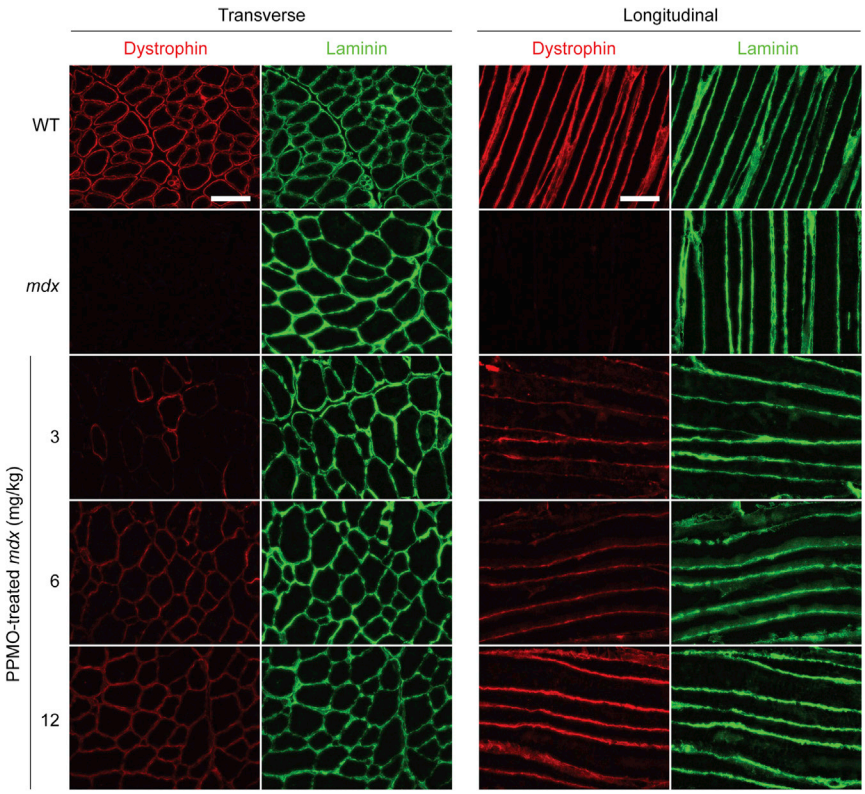

Figure 5. Distribution of sarcolemmal dystrophin expression in PPMO-treated *mdx* mice

Representative dystrophin immunofluorescence images of TA muscle sections in both transverse and longitudinal orientations for *mdx* mice treated with a single dose of PPMO (at 3, 6, or 12 mg/kg doses). Untreated WT and *mdx* samples were analyzed in parallel as controls. Sections were co-stained for laminin to delineate myofiber boundaries. Images were taken at 20× magnification and scale bars represent 100 μm.

could be utilized for diagnostic purposes.[40] The data contained in this study provide evidence that AFM might also be suitable for assessing the effectiveness of therapeutic interventions for DMD (Figure 6), although invasive biopsy collection is still required.

Notably, in this study, serum CK arguably performed better than the ex-myomiRs. CK is known to be highly variable in patients and affected by a number of confounding factors (e.g., exercise,[51,52] age,[53] race,[54] and drugs such as statins[55]), which may not have an impact on serum myomiR levels, as has been reported by others.[19] Furthermore, we previously observed that serum myomiR levels in human serum provided very high predictive power for distinguishing between DMD and healthy individuals (AUC > 0.99 for miR-206-3p, n = 28/16 DMD patients/healthy controls).[18] An important consideration is that the measurement of serum miRNA biomarkers requires multiple processing steps (i.e., RNA extraction, RT, qPCR amplification), whereas serum CK can be measured directly by either ELISA or enzymatic activity assay. As such, serum miRNA measurements may be subject to a greater degree of technical variation, especially in a research laboratory setting.

In this study, we also aimed to address the suitability of the small-RNA TaqMan RT-qPCR method to distinguish between closely related myomiRs. This commercial technology has been extensively used in the study of miRNAs across many areas of biology and medicine, and was shown to provide excellent discrimination between members of the let-7 family of miRNAs (some of which differ by only a single nucleotide, which is not the 3' terminus).[39] However, our data clearly show that this product is incapable of distinguishing between miRNAs that differ only in their 3'-terminal nucleotide, such as miR-133a-3p and miR-133b-3p, and that the lack of discrimination occurs at the RT step (Figure 2). We note that a similar failure to distinguish between miR-133a and miR-133b was reported by Ikeda et al., although the exact method and procedures used are not clear.[56] This technical point is important, given that multiple studies have reported expression data for both of these miRNAs using this technology.[24,30,32,33,35,36,38] The present study emphasizes the importance of assay validation, and how it should not be assumed that commercial products are valid *a priori*.

In conclusion, we show that PPMO-mediated exon skipping results in dose-dependent dystrophin rescue and restoration of the biophysical properties of dystrophic muscle. Importantly, a within-fiber uniform pattern of dystrophin expression was observed at all dose levels. Serum myomiR levels were inversely correlated with dystrophin expression and myofiber stiffness, thereby providing support for their use as pharmacodynamic biomarkers in the context of DMD.

MATERIALS AND METHODS

Animal studies

All procedures were authorized by the UK Home Office (project license 30/2907) in accordance with the Animals (Scientific Procedures) Act 1986. Animals were housed under a 12:12 h light:dark cycle, with access to food and water *ad libitum*. Mice used were male WT C57 (C57BL/10ScSn) or dystrophic *mdx* (C57BL/10ScSn-*Dmd*^{mdx}/J).

PPMO

PPMO conjugates consisted of a peptide (Pip9b2, Ac-RXRRBRR FQILYRBRXRB-OH, where X is aminohexanoic acid and B is β-alanine) covalently attached to a PMO designed to induce skipping of *Dmd* exon 23 (Table S2). The peptide was synthesized by standard Fmoc solid-phase chemistry and conjugated to the PMO via the amine of the morpholine heterocycle at its 3' terminus, as described

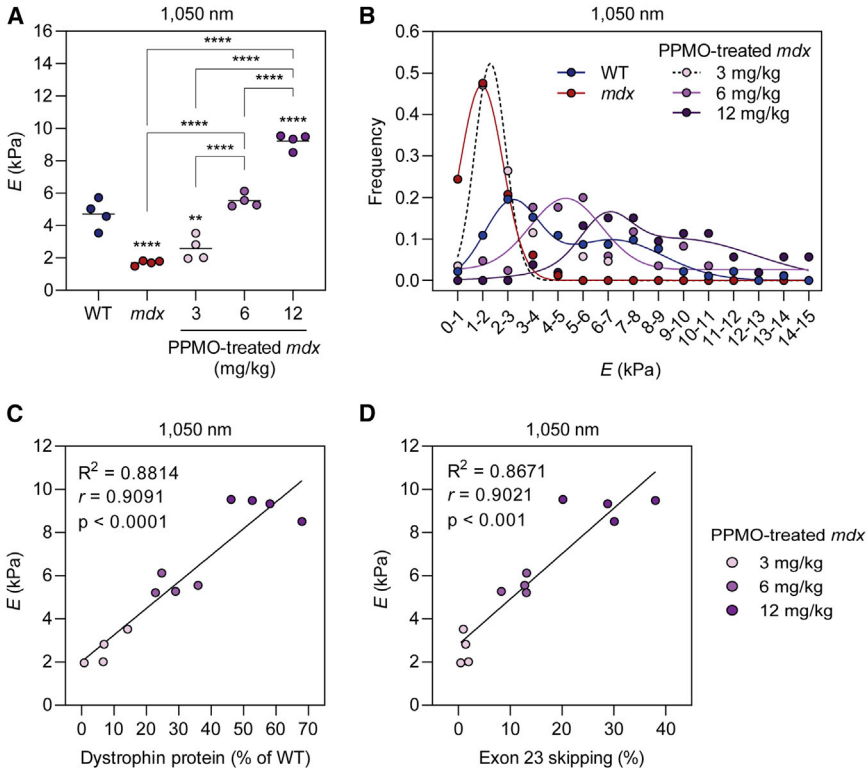

Figure 6. Dose-dependent changes in muscle stiffness following exon-skipping-mediated dystrophin rescue

Atomic force microscopy was performed to determine Young's modulus (*E*) calculated for an indentation depth of 1,050 nm in TA muscle explants from WT, *mdx*, and PPMO-treated *mdx* mice and plotted as (A) mean *E* value for each individual sample (representing 60 to 100 elasticity maps, depending on the sample group) and (B) the distribution of all determined *E* values. Mean values and individual sample data points are shown. Statistical significance was tested by one-way ANOVA and Bonferroni *post hoc* test. Statistical comparisons were made to the WT control group unless otherwise indicated, $^{**}p < 0.01$, $^{****}p < 0.0001$. Correlation analyses for Young's modulus versus (C) dystrophin protein expression and (D) *Dmd* exon 23 skipping in PPMO-treated *mdx* samples. Values were analyzed using linear regression and Spearman correlation analyses.

previously.[57] Conjugates were dissolved in sterile water and passed through 0.22 μm cellulose acetate filters.

Male *mdx* mice were injected with a single dose of PPMO conjugate (3, 6, or 12 mg/kg) in an equal volume of 150 μL 0.9% sterile saline via the tail vein at 8 weeks of age. Animals were sacrificed 2 weeks later (at 10 weeks of age) by escalating CO_2 concentration, and serum/muscle tissues were harvested.

TA muscles were macrodissected and flash-frozen in isopentane cooled on dry ice. Muscles were mounted on corks using Tissue-TEK O.C.T. Compound (VWR, Lutterworth, UK), to enable cryosectioning, and stored at −80°C.

Blood was harvested from the jugular vein and collected using Microvette CB 300 collection tubes (Sarstedt, Nümbrecht, Germany) as described previously.[58] Blood was incubated at 4°C for at least 2 h to facilitate clotting, and then cellular blood was pelleted by centrifugation at 10,000 *g* for 5 min. The serum supernatant was transferred to a fresh microcentrifuge tube and samples were stored at −80°C until ready for analysis.

Western blot

TA muscles were homogenized in modified RIPA buffer (50 mM Tris [pH 8], 150 mM NaCl, 1% IGEPAL CA-630, 0.5% sodium deoxycholate, 10% SDS, and 1× cOmplete protease inhibitor cocktail [Merck, Feltham, UK]) using a Precellys 24 tissue homogenizer (Bertin Instruments, Montigny-le-Bretonneux, France) (four cycles at 5,000 rpm for 30 s). Twenty micrograms of protein was mixed with NuPAGE sample reducing agent and NuPAGE LDS sample buffer and run on a NuPAGE 3% to 8% Tris-acetate gel (all Thermo Fisher Scientific, Abingdon, UK). Protein was electrotransferred onto a 0.45 μm polyvinylidene difluoride (PVDF) membrane for 1 h at 30 V, followed by 1 h at 100 V, and blocked with Odyssey blocking buffer (LI-COR Biosciences, Cambridge, UK) for 1 h at room temperature. Membranes were incubated with primary antibodies (Table S3) overnight in Odyssey blocking buffer supplemented with 0.1% Tween 20 at 4°C. Membranes were washed three times with PBST and then incubated with horseradish peroxidase (HRP)-conjugated secondary antibodies (Table S3) in Odyssey blocking buffer supplemented with 0.1% Tween 20 at room temperature for 1 h. Chemiluminescent signal was detected using Clarity Western ECL substrate (Bio-Rad, Watford, UK).

Exon 23 skipping RT-qPCR

Tissues were homogenized using a Precellys homogenizer (Bertin Instruments) (two cycles at 5,500 rpm for 30 s), and RNA was extracted using TRIzol reagent (Thermo Fisher Scientific) according to the manufacturer's instructions. cDNA was generated from 500 ng of total RNA using the High-Capacity cDNA Reverse Transcription Kit (Thermo Fisher Scientific) according to the manufacturer's instructions. The resulting cDNA was diluted 1:5 prior to analysis. cDNA was amplified using a StepOne Plus real-time PCR thermocycler with TaqMan Gene Expression Master Mix (both Thermo Fisher Scientific) using universal cycling conditions: 95°C for 10 min, followed by 45 cycles of 95°C for 15 s and 60°C for 1 min. All samples were analyzed in duplicate. Absolute quantification was performed by comparing samples with standard curves comprising serial dilutions of the full-length (unskipped) and Δ23 *Dmd* (skipped) DNA target templates (IDT, Leuven, Belgium). The degree of exon 23 skipping

was determined by calculating the percentage of skipped transcripts relative to the total (i.e., skipped + unskipped). Sequences of the RT-qPCR primers and probes are shown in Table S4.

Immunofluorescence

Fresh-frozen TA muscles were mounted onto corks with Tissue-TEK O.C.T. Compound and cryosectioned (8 μm) in transverse and longitudinal orientations. Sections were transferred onto SuperFrost Plus microslides (VWR), left to dry for 10 min at room temperature, and stored at −80°C until ready for analysis. Slides were air-dried, soaked in PBS for 10 min at room temperature, and then blocked in PBS supplemented with 20% fetal calf serum (FCS; Thermo Fisher Scientific) and 20% normal goat serum (NGS; MP Biomedicals, Eschwege, Germany) for 2 h at room temperature. Subsequently, the slides were incubated with primary antibodies in PBS supplemented with 20% FCS and 20% NGS for 2 h at room temperature. After being washed three times with PBS, the slides were incubated with fluorophore-conjugated secondary antibodies in PBS for 1 h at room temperature. The slides were then washed three times with PBS and mounted using Dako fluorescence mounting medium (Agilent, Didcot, UK). Details of all antibodies are shown in Table S3.

Serum biomarker analysis

Serum miRNA analysis was performed as described previously.[58,59] Briefly, RNA was extracted from 50 μL of blood serum using TRIzol LS (Thermo Fisher Scientific) according to the manufacturer's instructions, with minor modifications. A synthetic spike-in control oligonucleotide (i.e., cel-miR-39, 2.5 fmol, Table S2) was added at the phenolic extraction phase and mixed thoroughly. In addition, 150 μL nuclease-free water (Thermo Fisher Scientific) was added at the phenolic extraction phase to increase the volume of the aqueous phase after phase separation. RNA was precipitated using isopropanol, and 1 μL of RNase-free glycogen (Roche, Welwyn Garden City, UK) was added to each sample as an inert carrier to assist RNA recovery. Pellets were air-dried, and then the RNA was resuspended in 30 μL nuclease-free water, and the samples were incubated at 55°C for 10 min. Samples were stored at −80°C until ready for analysis. RT was performed with the TaqMan MicroRNA Reverse Transcription Kit (Thermo Fisher Scientific) according to the manufacturer's instructions, using 10 μL of each RNA sample. RT reactions were performed with miRNA-specific stem-loop primers as appropriate. The resulting RT product was diluted 1:2 prior to analysis, and 2 μL of cDNA was added per 20 μL qPCR. cDNA was amplified as described above. Data were normalized to cel-miR-39[59] and analyzed using the Pfaffl method.[60] Details of small-RNA TaqMan assays are provided in Table S5.

Serum CK analysis was performed as a service at the MRC Harwell Institute (Oxford, UK).

Atomic force microscopy nanoindentation assay

Mouse muscles were stored under liquid nitrogen in DMEM supplemented with 10% DMSO following the protocol published elsewhere.[40] One hour before AFM measurements, muscles were thawed at room temperature by placing them in a Petri dish filled with DMEM (Sigma-Aldrich, Burlington, MA, USA). Afterward, they were washed twice in DMEM (for 2 min each time). The muscles were next removed from the medium, and the bottom part was gently dried with filter paper, followed by gluing them onto a glass coverslip using two 0.5 μL droplets of cyanoadhesive placed at both extremities as described previously.[41] The muscle sample was immediately immersed in DMEM, and AFM measurements were performed (no longer than 3 h per individual muscle).

Measurements of the mechanical properties of muscles were carried out using an atomic force microscope (Xe120, Park Systems, Korea) equipped with a liquid cell sitting on a piezoelectric scanner with an xy range of 100 × 100 μm. AFM worked in a force spectroscopy mode that allows recording an approach and retracting the AFM probe (i.e., cantilever) using a separate piezoelectric scanner with a z range of 25 μm. Cantilevers were silicon nitride cantilevers of the ORC-8 (Bruker) type characterized by a nominal resonant frequency of 18 kHz, open angle of 36°, and nominal spring constant of 0.1 N/m. The spring constant of the cantilevers was calibrated using the Sader method.[61] It ranged from 0.101 to 0.110 N/m. Force curves, i.e., dependencies between cantilever deflection and relative sample position, were recorded to estimate the elastic properties of muscles. Force curves were recorded in 36 positions (a grid of 6 × 6 pixels was set). For each muscle sample, 28–31 maps were recorded (in total, 1,008 to 1,116 force curves were analyzed). Measurements were acquired at an approach and retract speed of 8 μm/s. Calibration curves (curves recorded on a stiff, non-deformable surface) were collected from the measurements of a silicon nitride rectangular chip glued at the muscle height level.

The contact mechanics model analyzes the relationship between the load force and the indentation. In the AFM, to obtain indentation values, force curves recorded on a stiff, non-deformable surface (here, glass coverslip) were subtracted from force curves collected on a muscle sample. The resulting force versus indentation curves were fitted with the Hertz-Sneddon contact mechanics assuming that the indenting AFM probe can be modeled as a cone.[62] For such a probe, the relation between the load force F and the resulting indentation depth δ is:

$$F = \frac{2.\tan\theta}{\pi}.\frac{E_{muscle}}{1-\nu^2}.\delta^2,$$

where θ is the open angle of the probing cone (here, 36°), ν is Poisson's ratio defining the compressibility of the studied material (here, $\nu = 0.5$ because cells are incompressible), and E_{muscle} is Young's (elastic) modulus of the studied muscle sample. Young's modulus was determined at three indentation depths, i.e., 250, 500, and 1,050 nm.

Statistics

Statistical analyses were performed using GraphPad Prism v.9 (GraphPad Software, La Jolla, CA, USA). Differences between groups

were compared using one-way ANOVA and Bonferroni *post hoc* test. Differences were considered significant at the $p < 0.05$ level. Other analyses performed in GraphPad were the Shapiro-Wilk and Kolmogorov-Smirnov tests for normality, linear regression, non-linear regression (Gaussian and sum of two Gaussian), and Spearman correlation analysis. Data were tested for outliers using Grubb's test, after which one sample in the 12 mg/kg group (which exhibited extremely high biomarker levels) was removed from all analyses. Heatmaps were produced using TMeV (The Institute for Genomic Research, Rockville, MD, USA).[63]

Data availability statement

All relevant data are included in the article. Raw data are available on request.

SUPPLEMENTAL INFORMATION

Supplemental information can be found online at https://doi.org/10.1016/j.omtn.2022.08.033.

ACKNOWLEDGMENTS

K.C. is supported by a doctoral studentship from the Clarendon Fund in partnership with the Medical Research Council (MRC) and the Juel-Jenson Scholarship from St Cross College, Oxford. This work was funded by an MRC Programme Grant awarded to M.J.A.W.

AUTHOR CONTRIBUTIONS

T.C.R., Y.L., and M.J.A.W. conceived the study. K.C., J.O., J.A., M.L., N.A., A.M.L.C-S., G.M., and Y.L. performed experiments and acquired data. T.C.R., Y.L., M.L., and M.J.A.W. supervised the work. K.C., J.O., and T.C.R. wrote the first draft of the manuscript. All authors contributed to the final draft of the manuscript.

DECLARATION OF INTERESTS

M.J.A.W. is a founder, shareholder, and consultant for PepGen Ltd, a biotech company that aims to commercialize PPMO technology.

REFERENCES

1. Hoffman, E.P., Brown, R.H., Jr., and Kunkel, L.M. (1987). Dystrophin: the protein product of the Duchenne muscular dystrophy locus. Cell *51*, 919–928.
2. Petrof, B.J., Shrager, J.B., Stedman, H.H., Kelly, A.M., and Sweeney, H.L. (1993). Dystrophin protects the sarcolemma from stresses developed during muscle contraction. Proc. Natl. Acad. Sci. USA *90*, 3710–3714.
3. Ervasti, J.M., and Campbell, K.P. (1993). A role for the dystrophin-glycoprotein complex as a transmembrane linker between laminin and actin. J. Cell Biol. *122*, 809–823.
4. Aartsma-Rus, A., Fokkema, I., Verschuuren, J., Ginjaar, I., van Deutekom, J., van Ommen, G.-J., and den Dunnen, J.T. (2009). Theoretic applicability of antisense-mediated exon skipping for Duchenne muscular dystrophy mutations. Hum. Mutat. *30*, 293–299.
5. Roberts, T.C., Langer, R., and Wood, M.J.A. (2020). Advances in oligonucleotide drug delivery. Nat. Rev. Drug Discov. *19*, 673–694.
6. Charleston, J.S., Schnell, F.J., Dworzak, J., Donoghue, C., Lewis, S., Chen, L., Young, G.D., Milici, A.J., Voss, J., DeAlwis, U., et al. (2018). Eteplirsen treatment for Duchenne muscular dystrophy: exon skipping and dystrophin production. Neurology *90*, e2146–e2154.
7. Komaki, H., Nagata, T., Saito, T., Masuda, S., Takeshita, E., Sasaki, M., Tachimori, H., Nakamura, H., Aoki, Y., and Takeda, S. (2018). Systemic administration of the antisense oligonucleotide NS-065/NCNP-01 for skipping of exon 53 in patients with Duchenne muscular dystrophy. Sci. Transl. Med. *10*, eaan0713.
8. Godfrey, C., Muses, S., McClorey, G., Wells, K.E., Coursindel, T., Terry, R.L., Betts, C., Hammond, S., O'Donovan, L., Hildyard, J., et al. (2015). How much dystrophin is enough: the physiological consequences of different levels of dystrophin in the mdx mouse. Hum. Mol. Genet. *24*, 4225–4237.
9. van Westering, T.L.E., Lomonosova, Y., Coenen-Stass, A.M.L., Betts, C.A., Bhomra, A., Hulsker, M., Clark, L.E., McClorey, G., Aartsma-Rus, A., van Putten, M., et al. (2020). Uniform sarcolemmal dystrophin expression is required to prevent extracellular microRNA release and improve dystrophic pathology. J. Cachexia Sarcopenia Muscle *11*, 578–593.
10. Torelli, S., Scaglioni, D., Sardone, V., Ellis, M.J., Domingos, J., Jones, A., Feng, L., Chambers, D., Eastwood, D.M., Leturcq, F., et al. (2021). High-throughput digital image analysis reveals distinct patterns of dystrophin expression in dystrophinopathy patients. J. Neuropathol. Exp. Neurol. *80*, 955–965.
11. Aartsma-Rus, A., and Spitali, P. (2015). Circulating biomarkers for duchenne muscular dystrophy. J. Neuromuscul. Dis. *2*, S49–S58.
12. Coenen-Stass, A.M.L., Wood, M.J.A., and Roberts, T.C. (2017). Biomarker potential of extracellular miRNAs in duchenne muscular dystrophy. Trends Mol. Med. *23*, 989–1001.
13. Chen, J.-F., Tao, Y., Li, J., Deng, Z., Yan, Z., Xiao, X., and Wang, D.-Z. (2010). microRNA-1 and microRNA-206 regulate skeletal muscle satellite cell proliferation and differentiation by repressing Pax7. J. Cell Biol. *190*, 867–879.
14. Chen, J.-F., Mandel, E.M., Thomson, J.M., Wu, Q., Callis, T.E., Hammond, S.M., Conlon, F.L., and Wang, D.-Z. (2006). The role of microRNA-1 and microRNA-133 in skeletal muscle proliferation and differentiation. Nat. Genet. *38*, 228–233.
15. Kim, H.K., Lee, Y.S., Sivaprasad, U., Malhotra, A., and Dutta, A. (2006). Muscle-specific microRNA miR-206 promotes muscle differentiation. J. Cell Biol. *174*, 677–687.
16. Boutz, P.L., Chawla, G., Stoilov, P., and Black, D.L. (2007). MicroRNAs regulate the expression of the alternative splicing factor nPTB during muscle development. Genes Dev. *21*, 71–84.
17. Cacchiarelli, D., Legnini, I., Martone, J., Cazzella, V., D'Amico, A., Bertini, E., and Bozzoni, I. (2011). miRNAs as serum biomarkers for Duchenne muscular dystrophy. EMBO Mol. Med. *3*, 258–265.
18. Coenen-Stass, A.M.L., Sork, H., Gatto, S., Godfrey, C., Bhomra, A., Krjutškov, K., Hart, J.R., Westholm, J.O., O'Donovan, L., Roos, A., et al. (2018). Comprehensive RNA-sequencing analysis in serum and muscle reveals novel small RNA signatures with biomarker potential for DMD. Mol. Ther. Nucleic Acids *13*, 1–15.
19. Mizuno, H., Nakamura, A., Aoki, Y., Ito, N., Kishi, S., Yamamoto, K., Sekiguchi, M., Takeda, S., and Hashido, K. (2011). Identification of muscle-specific microRNAs in serum of muscular dystrophy animal models: promising novel blood-based markers for muscular dystrophy. PLoS One *6*, e18388.
20. Roberts, T.C., Blomberg, K.E.M., McClorey, G., El Andaloussi, S., Godfrey, C., Betts, C., Coursindel, T., Gait, M.J., Smith, C.I.E., and Wood, M.J.A. (2012). Expression analysis in multiple muscle groups and serum reveals complexity in the MicroRNA transcriptome of the mdx mouse with implications for therapy. Mol. Ther. Nucleic Acids *1*, e39.
21. Roberts, T.C., Godfrey, C., McClorey, G., Vader, P., Briggs, D., Gardiner, C., Aoki, Y., Sargent, I., Morgan, J.E., and Wood, M.J.A. (2013). Extracellular microRNAs are dynamic non-vesicular biomarkers of muscle turnover. Nucleic Acids Res. *41*, 9500–9513.
22. van Westering, T.L.E., Johansson, H.J., Hanson, B., Coenen-Stass, A.M.L., Lomonosova, Y., Tanihata, J., Motohashi, N., Yokota, T., Takeda, S., Lehtiö, J., et al. (2020). Mutation-independent proteomic signatures of pathological progression in murine models of duchenne muscular dystrophy. Mol. Cell. Proteomics *19*, 2047–2068.
23. Goyenvalle, A., Babbs, A., Wright, J., Wilkins, V., Powell, D., Garcia, L., and Davies, K.E. (2012). Rescue of severely affected dystrophin/utrophin-deficient mice through scAAV-U7snRNA-mediated exon skipping. Hum. Mol. Genet. *21*, 2559–2571.
24. Vignier, N., Amor, F., Fogel, P., Duvallet, A., Poupiot, J., Charrier, S., Arock, M., Montus, M., Nelson, I., Richard, I., et al. (2013). Distinctive serum miRNA profile in mouse models of striated muscular pathologies. PLoS One *8*, e55281.

25. Jeanson-Leh, L., Lameth, J., Krimi, S., Buisset, J., Amor, F., Le Guiner, C., Barthélémy, I., Servais, L., Blot, S., Voit, T., and Israeli, D. (2014). Serum profiling identifies novel muscle miRNA and cardiomyopathy-related miRNA biomarkers in Golden Retriever muscular dystrophy dogs and Duchenne muscular dystrophy patients. Am. J. Pathol. *184*, 2885–2898.

26. Coenen-Stass, A.M.L., McClorey, G., Manzano, R., Betts, C.A., Blain, A., Saleh, A.F., Gait, M.J., Lochmüller, H., Wood, M.J.A., and Roberts, T.C. (2015). Identification of novel, therapy-responsive protein biomarkers in a mouse model of Duchenne muscular dystrophy by aptamer-based serum proteomics. Sci. Rep. *5*, 17014.

27. Toivonen, J.M., Manzano, R., Oliván, S., Zaragoza, P., García-Redondo, A., and Osta, R. (2014). MicroRNA-206: a potential circulating biomarker candidate for amyotrophic lateral sclerosis. PLoS One *9*, e89065.

28. Catapano, F., Zaharieva, I., Scoto, M., Marrosu, E., Morgan, J., Muntoni, F., and Zhou, H. (2016). Altered levels of MicroRNA-9, -206, and -132 in spinal muscular atrophy and their response to antisense oligonucleotide therapy. Mol. Ther. Nucleic Acids *5*, e331.

29. Perfetti, A., Greco, S., Bugiardini, E., Cardani, R., Gaia, P., Gaetano, C., Meola, G., and Martelli, F. (2014). Plasma microRNAs as biomarkers for myotonic dystrophy type 1. Neuromuscul. Disord. *24*, 509–515.

30. Koutsoulidou, A., Kyriakides, T.C., Papadimas, G.K., Christou, Y., Kararizou, E., Papanicolaou, E.Z., and Phylactou, L.A. (2015). Elevated muscle-specific miRNAs in serum of myotonic dystrophy patients relate to muscle disease progress. PLoS One *10*, e0125341.

31. van Putten, M., Hulsker, M., Nadarajah, V.D., van Heiningen, S.H., van Huizen, E., van Iterson, M., Admiraal, P., Messemaker, T., den Dunnen, J.T., 't Hoen, P.A.C., and Aartsma-Rus, A. (2012). The effects of low levels of dystrophin on mouse muscle function and pathology. PLoS One *7*, e31937.

32. Hightower, R.M., Samani, A., Reid, A.L., English, K.G., Lopez, M.A., Doyle, J.S., Conklin, M.J., Schneider, D.A., Bamman, M.M., Widrick, J.J., et al. (2021). miR-486 is an epigenetic modulator of Duchenne muscular dystrophy pathologies. Preprint at bioRxiv. https://doi.org/10.1101/2021.06.14.448387.

33. Zaharieva, I.T., Calissano, M., Scoto, M., Preston, M., Cirak, S., Feng, L., Collins, J., Kole, R., Guglieri, M., Straub, V., et al. (2013). Dystromirs as serum biomarkers for monitoring the disease severity in duchenne muscular dystrophy. PLoS One *8*, e80263.

34. Zhang, J., Meng, Q., Zhong, J., Zhang, M., Qin, X., Ni, X., Ma, J., He, Y., Zeng, D., and Lan, D. (2020). Serum MyomiRs as biomarkers for female carriers of duchenne/becker muscular dystrophy. Front. Neurol. *11*, 617878.

35. Perfetti, A., Greco, S., Cardani, R., Fossati, B., Cuomo, G., Valaperta, R., Ambrogi, F., Cortese, A., Botta, A., Mignarri, A., et al. (2016). Validation of plasma microRNAs as biomarkers for myotonic dystrophy type 1. Sci. Rep. *6*, 38174.

36. Koutsoulidou, A., Photiades, M., Kyriakides, T.C., Georgiou, K., Prokopi, M., Kapnisis, K., Lusakowska, A., Nearchou, M., Christou, Y., Papadimas, G.K., et al. (2017). Identification of exosomal muscle-specific miRNAs in serum of myotonic dystrophy patients relating to muscle disease progress. Hum. Mol. Genet. *26*, 3285–3302.

37. Mytidou, C., Koutsoulidou, A., Katsioloudi, A., Prokopi, M., Kapnisis, K., Michailidou, K., Anayiotos, A., and Phylactou, L.A. (2021). Muscle-derived exosomes encapsulate myomiRs and are involved in local skeletal muscle tissue communication. Faseb. J. *35*, e21279.

38. Koutsoulidou, A., Mastroyiannopoulos, N.P., Furling, D., Uney, J.B., and Phylactou, L.A. (2011). Expression of miR-1, miR-133a, miR-133b and miR-206 increases during development of human skeletal muscle. BMC Dev. Biol. *11*, 34.

39. Chen, C., Ridzon, D.A., Broomer, A.J., Zhou, Z., Lee, D.H., Nguyen, J.T., Barbisin, M., Xu, N.L., Mahuvakar, V.R., Andersen, M.R., et al. (2005). Real-time quantification of microRNAs by stem-loop RT-PCR. Nucleic Acids Res. *33*, e179.

40. Van Zwieten, R.W., Puttini, S., Lekka, M., Witz, G., Gicquel-Zouida, E., Richard, I., Lobrinus, J.A., Chevalley, F., Brune, H., Dietler, G., et al. (2014). Assessing dystrophies and other muscle diseases at the nanometer scale by atomic force microscopy. Nanomedicine *9*, 393–406.

41. Puttini, S., Lekka, M., Dorchies, O.M., Saugy, D., Incitti, T., Ruegg, U.T., Bozzoni, I., Kulik, A.J., and Mermod, N. (2009). Gene-mediated restoration of normal myofiber elasticity in dystrophic muscles. Mol. Ther. *17*, 19–25.

42. Hanson, B., Stenler, S., Ahlskog, N., Chwalenia, K., Svrzikapa, N., Coenen-Stass, A.M.L., Weinberg, M.S., Wood, M.J.A., and Roberts, T.C. (2022). Non-uniform dystrophin re-expression after CRISPR-mediated exon excision in the dystrophin/utrophin double-knockout mouse model of DMD. Preprint at bioRxiv. https://doi.org/10.1101/2022.01.25.477678.

43. Hanson, B., Wood, M.J.A., and Roberts, T.C. (2021). Molecular correction of Duchenne muscular dystrophy by splice modulation and gene editing. RNA Biol. *18*, 1048–1062.

44. Israeli, D., Poupiot, J., Amor, F., Charton, K., Lostal, W., Jeanson-Leh, L., and Richard, I. (2016). Circulating miRNAs are generic and versatile therapeutic monitoring biomarkers in muscular dystrophies. Sci. Rep. *6*, 28097.

45. Holmberg, J., Alajbegovic, A., Gawlik, K.I., Elowsson, L., and Durbeej, M. (2014). Laminin α2 chain-deficiency is associated with microRNA deregulation in skeletal muscle and plasma. Front. Aging Neurosci. *6*, 155.

46. Li, J., Fredericks, M., Cannell, M., Wang, K., Sako, D., Maguire, M.C., Grenha, R., Liharska, K., Krishnan, L., Bloom, T., et al. (2021). ActRIIB:ALK4-Fc alleviates muscle dysfunction and comorbidities in murine models of neuromuscular disorders. J. Clin. Invest. *131*, 138634.

47. Tinsley, J., Deconinck, N., Fisher, R., Kahn, D., Phelps, S., Gillis, J.M., and Davies, K. (1998). Expression of full-length utrophin prevents muscular dystrophy in mdx mice. Nat. Med. *4*, 1441–1444.

48. Coenen-Stass, A.M.L., Betts, C.A., Lee, Y.F., Mäger, I., Turunen, M.P., El Andaloussi, S., Morgan, J.E., Wood, M.J.A., and Roberts, T.C. (2016). Selective release of muscle-specific, extracellular microRNAs during myogenic differentiation. Hum. Mol. Genet. *25*, 3960–3974.

49. Coenen-Stass, A.M.L., Pauwels, M.J., Hanson, B., Martin Perez, C., Conceição, M., Wood, M.J.A., Mäger, I., and Roberts, T.C. (2019). Extracellular microRNAs exhibit sequence-dependent stability and cellular release kinetics. RNA Biol. *16*, 696–706.

50. Gnocchi, V.F., Scharner, J., Huang, Z., Brady, K., Lee, J.S., White, R.B., Morgan, J.E., Sun, Y.-B., Ellis, J.A., and Zammit, P.S. (2011). Uncoordinated transcription and compromised muscle function in the Lmna-null mouse model of emery-dreifuss muscular dystrophy. PLoS One *6*, e16651.

51. Nicholson, G.A., Morgan, G.J., Meerkin, M., Strauss, E.R., and McLeod, J.G. (1986). The effect of aerobic exercise on serum creatine kinase activities. Muscle Nerve *9*, 820–824.

52. Baird, M.F., Graham, S.M., Baker, J.S., and Bickerstaff, G.F. (2012). Creatine-kinase- and exercise-related muscle damage implications for muscle performance and recovery. J. Nutr. Metab. *2012*, 960363.

53. Zatz, M., Rapaport, D., Vainzof, M., Passos-Bueno, M.R., Bortolini, E.R., Pavanello, R. de C., and Peres, C.A. (1991). Serum creatine-kinase (CK) and pyruvate-kinase (PK) activities in Duchenne (DMD) as compared with Becker (BMD) muscular dystrophy. J. Neurol. Sci. *102*, 190–196.

54. Wong, E.T., Cobb, C., Umehara, M.K., Wolff, G.A., Haywood, L.J., Greenberg, T., and Shaw, S.T. (1983). Heterogeneity of serum creatine kinase activity among racial and gender groups of the population. Am. J. Clin. Pathol. *79*, 582–586.

55. Dugué, A., Bagheri, H., Lapeyre-Mestre, M., Tournamille, J.F., Sailler, L., Dedieu, G., Salvayre, R., Thouvenot, J.P., Massip, P., and Montastruc, J.L. (2004). Detection and incidence of muscular adverse drug reactions: a prospective analysis from laboratory signals. Eur. J. Clin. Pharmacol. *60*, 285–292.

56. Ikeda, S., He, A., Kong, S.W., Lu, J., Bejar, R., Bodyak, N., Lee, K.-H., Ma, Q., Kang, P.M., Golub, T.R., and Pu, W.T. (2009). MicroRNA-1 negatively regulates expression of the hypertrophy-associated calmodulin and Mef2a genes. Mol. Cell Biol. *29*, 2193–2204.

57. Betts, C., Saleh, A.F., Arzumanov, A.A., Hammond, S.M., Godfrey, C., Coursindel, T., Gait, M.J., and Wood, M.J. (2012). Pip6-PMO, A new generation of peptide-oligonucleotide conjugates with improved cardiac exon skipping activity for DMD treatment. Mol. Ther. Nucleic Acids *1*, e38.

58. Roberts, T.C., Coenen-Stass, A.M.L., Betts, C.A., and Wood, M.J.A. (2014). Detection and quantification of extracellular microRNAs in murine biofluids. Biol. Proced. Online *16*, 5.

59. Roberts, T.C., Coenen-Stass, A.M.L., and Wood, M.J.A. (2014). Assessment of RT-qPCR normalization strategies for accurate quantification of extracellular microRNAs in murine serum. PLoS One *9*, e89237.

60. Pfaffl, M.W. (2001). A new mathematical model for relative quantification in real-time RT-PCR. Nucleic Acids Res. *29*, e45.

61. Sader, J.E., Larson, I., Mulvaney, P., and White, L.R. (1995). Method for the calibration of atomic force microscope cantilevers. Rev. Sci. Instrum. *66*, 3789–3798.

62. Sneddon, I.N. (1965). The relation between load and penetration in the axisymmetric boussinesq problem for a punch of arbitrary profile. Int. J. Eng. Sci. *3*, 47–57.

63. Saeed, A.I., Sharov, V., White, J., Li, J., Liang, W., Bhagabati, N., Braisted, J., Klapa, M., Currier, T., Thiagarajan, M., et al. (2003). TM4: a free, open-source system for microarray data management and analysis. Biotechniques *34*, 374–378.